

Article

The Influence of the Textural Characteristics of the Hierarchical Porous Carbons on the Removal of Lead and Cadmium Ions from Aqueous Solution

Turki N. Baroud 

Department of Mechanical Engineering, King Fahd University of Petroleum and Mineral, Dhahran 31261, Saudi Arabia; turkibaroud@kfupm.edu.sa

Abstract: Developing efficient adsorbent materials for water treatment is deemed as one of the key solutions towards mitigating the contaminated water problem. Herein, several Hierarchical Porous Carbons (HPCs) with large mesopore volumes (up to 3 cm³/g) and a wide range of BET surface areas (747–1037 m²/g) were synthesized, and their heavy metal removal behaviors were investigated. Specifically, simulated lead and cadmium aqueous solutions were used to investigate the HPCs adsorption performance towards lead and cadmium removal. All the HPCs demonstrated high affinities towards lead removal compared with cadmium. Additionally, a systematic investigation was carried out to understand the structure–performance relationships for the HPCs. Interestingly, varying the adsorbent pore structure leads to different adsorbent behavior for lead compared with cadmium. The textural characteristics of the HPCs have a limited effect on the removal of cadmium ions. Accordingly, to expedite cadmium removal from aqueous samples, factors other than textural characteristics (i.e., surface chemistry) might enhance the removal process. Conversely, the removal of lead ions can be significantly controlled by the HPCs pore structure. HPC1221 (with 17 nm mesopore size, 2.8 cm³/g pore volume, 907 m²/g) showed the maximum adsorption capacity value of 12.32 mg/g for Cd²⁺ and 89 mg/g for Pb²⁺ compared to other HPCs. The significant adsorption parameters were evaluated using the response surface methodology (RSM) design. We believe that the reported insights for the structure–performance relationships will be useful for better designing highly efficient adsorbent materials.



Citation: Baroud, T.N. The Influence of the Textural Characteristics of the Hierarchical Porous Carbons on the Removal of Lead and Cadmium Ions from Aqueous Solution. *Sustainability* **2021**, *13*, 5790. <https://doi.org/10.3390/su13115790>

Academic Editors:
Ihsanullah Ihsanullah, Mu Naushad
and Muhammad Bilal

Received: 10 April 2021
Accepted: 18 May 2021
Published: 21 May 2021

Publisher's Note: MDPI stays neutral with regard to jurisdictional claims in published maps and institutional affiliations.



Copyright: © 2021 by the author. Licensee MDPI, Basel, Switzerland. This article is an open access article distributed under the terms and conditions of the Creative Commons Attribution (CC BY) license (<https://creativecommons.org/licenses/by/4.0/>).

Keywords: hierarchical porous carbons; heavy metals removal; water treatment; porosity; adsorption

1. Introduction

The shortage and decline in clean water is a critical issue and a threat to many communities in the developing world. The search for feasible solutions to provide and secure sustainable access to clean water has become a priority, especially with a substantial increase in water demands because of the expanding population and industrialization. Hence, the water crisis has been viewed in the last few years as one of the major global risks. Data from the world health organization WHO show that more than 2 billion people do not have access to clean drinking water [1]. Unfortunately, less than 0.3% of fresh water on our planet is accessible and the remainder is either salty water (around 98%) or non-accessible freshwater [2]. To overcome this challenge, several water treatment approaches have been developed and utilized for providing safe drinking water to people. The pollution of these available water sources with heavy metals either through anthropogenic and/or man-made activity has served to compound the water crisis problem [3].

Heavy metals are persistent environmental pollutants that are toxic, carcinogenic and can bioaccumulate in living organisms. There are many types of heavy metals that can be found in wastewater such as zinc, lead, copper, cadmium, nickel, chromium and iron, all of which can cause risks for human health and the environment. For instance, human exposure to cadmium at trace level is often associated with renal dysfunction,

and mortality has been reported at elevated levels [4]. Cadmium has an affinity for sulfhydryl groups of proteins for which it competes with Zn(II) in biological systems and is known as a human carcinogen [5,6]. Furthermore, lead can impair the functioning of the human blood, kidney, and brain. High concentrations of lead can result in kidney and liver damage, cognitive impairment, anemia, and toxicity to the reproductive system [7]. Despite their toxic effect on humans and the environment, both lead and cadmium are used in a wide range of applications [8–10]. For example, lead metals are used in the nuclear industry as a radiation shield and as a component in metal alloys in the building industry. Additionally, lead metal is used in the textile industry, metal processing, and finishing, as solders with tin, storage batteries, and lead pigments. There are many ways in which humans can be exposed to lead ions, such as lead dust from lead paints and lead ions from lead pipes. Cadmium is used for the manufacturing of coatings, photovoltaic devices, and batteries. The release of cadmium into the environment can occur through mining, smelting, and the incineration of municipal waste [11]. The toxic effects of these two metals have made the World Health Organization (WHO) set the maximum permissible level of lead and cadmium in the discharged effluents into aquatic water to 0.01 and 0.003 mg L⁻¹, respectively. Additionally, the US Environmental Protection Agency (USEPA) discharge limit for lead and cadmium in effluents is 0.005 and 0.002 mg L⁻¹, respectively [11,12].

Considering this, several approaches have been proposed and utilized in mitigating heavy metal pollution. The conventional and widely used approaches for heavy metal removal include (i) chemical precipitation as sulfides, carbonates or hydroxides [13–16]; (ii) membrane-based processes [17,18]; (iii) electrochemical treatment technologies [19]; (vi) adsorption [20,21], etc. All these approaches and others have their limitations. For instance, while the use of chemical precipitation is deemed as an efficient technique, sludge production and sludge disposal can be considered the major disadvantages of this approach. Moreover, membrane technology can offer high separation selectivity with low-pressure requirements, but this approach suffers from membrane fouling during adsorption in addition to low permeate flux and the production of large volume of rejected residuals. Electrodialysis can also offer high separation selectivity. However, the high operational cost due to the required energy and possible fouling are the main limitations to this approach [11]. On the other hand, the adsorption method is viewed as the most effective approach for aqueous heavy metal removal [22]. Its fundamental principle relies on the attachment of the target solute in the aqueous phase (the adsorbates) to the surface of the adsorbent material. At the solution–adsorbent surface interface, the solute can attach to the adsorbent surface either physically (physisorption) or chemically (chemisorption) depending on the surface properties of the adsorbent material. Hence, the surface properties of the adsorbent, which include the textural and chemical characteristics (functional groups), play a significant role in its application for aqueous pollutant removal. Up to now, a wide range of materials such as zeolite [23–25], alumina and alumina composites [26,27], flash ash [28–30], metal oxides [30], nanocomposites [31], carbon nanotubes [32], and activated carbon [33–41] have been used as adsorbent materials for the heavy metal removal. Each adsorbent has its own advantages and disadvantages. For example, despite the fact that carbon nanotubes (CNTs) have a high adsorption capacity for heavy metals (especially functionalized CNTs), the cost of CNTs has been a barrier to their commercial use. Additionally, the release of CNTs into aquatic water can potentially lead to environmental and health problems [42]. Notably, CNTs are not the only adsorbent materials with potential toxic effects. Metal and metal oxide nanomaterials can also be toxic when released or leached into the environment. Thus, several syntheses and functionalization approaches have been utilized to reduce the toxicity of the utilized adsorbent materials [43]. Activated carbon (AC) has been widely utilized for water treatment purposes, especially for heavy metal removal due to its characteristic high surface properties. Compared with other adsorbent materials, activated carbons often possess high surface area and porous structure that can enhance the heavy metal uptake. The mechanism of heavy metal adsorption by ACs has been ascribed to either electrostatic or non-electrostatic interactions. The electrostatic

interactions rely on several factors, including the charge density of the surface of the carbon, ionic strength of the electrolyte, and the chemical characteristics of the adsorbate. Hence, the electrostatic integrations could be either attractive or repulsive. On the other hand, non-electrostatic interactions such as hydrogen bonding, hydrophobic interactions, and van der Waals forces are always attractive [44].

Great efforts are being taken by many researchers to produce activated carbon ACs from abundant low-cost carbonaceous raw and waste materials such as peanut shells, straw, pistachio shells [45], and electronic-based materials [46]. Unfortunately, most of the waste-based materials, in addition to the natural adsorbent, often demonstrate several drawbacks, including low contaminant removal capacity, lack of interaction specificity, and environmental instability [47].

Up to now, there are several modifications and treatment strategies that have been used to enhance the adsorption capacity of ACs. Some of the strategies include chemical and physical surface modification approaches [48–50]. Interestingly, a chemical surface modification that involves introducing weakly acidic surface groups has been found to be highly effective in increasing the sorption capacity and selectivity of ACs for trace heavy metal ions. A study has shown that surface modification of AC by increasing the oxygen-containing group can enhance cadmium uptake by a factor of 13 as compared with unmodified AC [51]. Similarly, Park et al. were able to show that surface modification of AC with anionic surfactant led to negatively charged carbons, which enhanced its adsorption capacities in proportion to the amount of surfactant introduced [52]. In addition, some of these modifications can result in slow intraparticle diffusion and more complicated regeneration procedures [51].

Besides the impact of chemical modifications on the adsorption capacity, pore matrices and surface area can also impact the adsorption of heavy metals. High surface areas of the activated carbons are the result of the abundant micropores within the carbon matrix, which theoretically can provide many active sites for the targeted ions to be attached and held. However, Brunauer, Emmett and Teller (BET) surface area does not always demonstrate a positive correlation with the specific capacity of the carbon materials. This has been associated with the fact that high values of BET surface area might have resulted from large fractions of non-accessible micropores. Hence, a portion of the calculated BET surface area will not be available for the ion adsorption process [53]. Reddy et al. compared the adsorption capacity of two activated carbons with similar surface areas [54]. They found that the activated carbon with a larger pore size demonstrated a higher adsorption capacity, which was ascribed to easier diffusion of the targeted molecules into the pore. Similarly, Tamai et al. found that the adsorbent's pore size distribution was an important factor for enhancing the adsorption performance [55].

Hierarchical porous carbons (HPCs) with multi levels of porosity have the potential to overcome the mass transfer issues that are commonly encountered in high surface area activated carbons with only a microporous structure. For many applications where the electrolyte/surface interface is a significant aspect (i.e., batteries, supercapacitors, and capacitive deionization technologies), hierarchical porous carbons have consistently out-performed other types of carbon structures (including the activated carbons) [56–59]. Although HPC is viewed as a promising structure in many applications, most of the reported synthesis procedures involve complicated steps and, most importantly, they lack the control and fine-tuning of the carbon pore structure. Specifically, wide pore size distribution and losing control of mesopore size resulted in limiting the possible utilizations of HPC for understanding the structure–performance relationships in heavy metal removal. The carbon synthesis procedure and the nature of the carbon precursors contribute significantly to the adsorption process [60]. Thus, to understand the role of pore structure during the adsorption process, it is important to compare the performance of the different carbons that were synthesized by using the same precursor and under similar synthesis conditions.

In this work, hierarchical porous carbon HPCs with controllable pore (size and volume), high surface area, and high mesopore fraction will be synthesized via the ice-templation approach using the same precursor and then used for aqueous heavy metals adsorption. The synthesized HPCs are expected to excel in the removal of heavy metals as they can provide easy pathways and open channels for the diffusion of the ions and consequently utilize the available surfaces. To our knowledge, this is the first time that tunable HPCs with a high fraction of mesopores and high surface area will be utilized for heavy metal removal. Notably, such a tunable HPC synthesis approach allows for a close and accurate investigation of the impact of textural characteristics on HPC removal behavior of HPCs toward heavy metals.

2. Experimental

Hierarchical Porous Carbons Synthesis

A series of HPCs were synthesized based on the previously reported procedure [61]. Optimum weight percentages of colloidal silica template/sucrose were mixed at room temperature until the sucrose completely dissolved in the solution. To create the macropores, the mixture solution was then frozen by thrusting it into liquid nitrogen and immediately transferred to a freeze dryer (0.0014 mBar, room temperature) for more than 72 h. To create mesopores, a silica-sucrose composite was carbonized at 1050 °C for 3 h (in a nitrogen environment) before removing the silica particles. The etching step was carried out at 80 °C in 3 M NaOH for at least 12 h. The carbon samples were denoted as follows: the last two digits represent the hard template silica/sucrose ratio, where the rest digit/s is associated with hard template silica size. For instance, HPC with silica/sucrose ratio 2/1 and 12 nm average silica size was denoted HPC1221.

3. HPCs Characterization

An ASAP2020 instrument was used to characterize the HPCs surface area and pore distribution using nitrogen adsorption and desorption isotherms under 77.3 K. Prior to the measurements, all the samples were degassed at 473 K for at least 12 h. Transmission Electron Microscopy (TEM) and Scanning Electron Microscopy (SEM) images of the synthesized HPCs were obtained to characterize the surface morphology of the samples. EDXS was used to investigate the elemental compositions of HPCs. The carbon surface was further analyzed by Raman spectroscopy (Renishaw InVia, excitation power of 10 mW at 514 nm).

4. Heavy Metals Removal Experiment

Chemicals and Instrumentation

Cadmium nitrate ($\text{Cd}(\text{NO}_3)_2 \cdot 4\text{H}_2\text{O}$), Lead nitrate ($\text{Pb}(\text{NO}_3)_2$), hydrochloric acid (HCl), and sodium hydroxide (NaOH) were supplied by Sigma-Aldrich chemicals (St. Louis, MO, USA) (>99% purity) and were used without further purification.

A standard stock solution of the metals was prepared according to the following procedure: 1 g/L Cd^{2+} stock solution was prepared by dissolving 2.744 g of cadmium nitrate in 1 L of 0.5 M nitric acid (HNO_3) solution. Similarly, a 1 g/L stock solution of Pb^{2+} was prepared by dissolving 1.6 g of lead nitrate in 1 liter of 0.5 M nitric acid. The working solutions were prepared by appropriate dilution of the stock solution using deionized water. Sample pH adjustment was performed with 0.1 M HCl and NaOH solutions. Cd^{2+} and Pb^{2+} concentrations were measured using the Atomic Absorption Spectrometer (AAS).

The performance of the prepared HPCs for Cd^{2+} and Pb^{2+} removal from aqueous samples was evaluated through the various adsorption experiments conducted.

In the initial stage, the effect of adsorption time variation (adsorption kinetics) for all the prepared HPCs was performed to evaluate the minimum time required for an effective adsorption process. These experiments were used for screening the best HPC sample, which was employed for subsequent adsorption experiments. For adsorption time experiments, a 100 mL solution of 100 mg/L initial concentration of Cd^{2+} and Pb^{2+} in both

single and binary solution systems was prepared. The prepared solution pH was kept at 5–6, and an adsorbent dosage of 1 g/L was utilized. During the adsorption experiments, the HPC samples were contacted with the prepared solutions in an Erlenmeyer flask and subsequently agitated with a rotary shaker. Samples were collected at different time intervals (30–1440 min), filtered, and analyzed for their residual concentration of Cd²⁺ and Pb²⁺.

The removal capacity of HPC was evaluated using the following Equation (1):

$$\text{Removal capacity} = (V (C_0 - C_t)/m) \quad (1)$$

where removal capacity is in (mg/g), V is the solution volume in (liter), and m is the adsorbent mass (g).

Furthermore, on employing the best HPC sample realized for the kinetic experiments, the effect of the significant adsorption factors that include initial concentration, pH, and adsorbent dosage were all investigated. For this purpose, a central composite experimental design (CCD) based on response surface methodology was considered. The chosen factors for the design were designated as follows, A—Initial concentration, B—adsorbent dosage, and C—pH. The experimental procedure adopted was similar to the one reported for the kinetic study. In basic terms, it involves contacting different amounts of the HPC with varying concentrations of the metals at different pH values in a 100 mL Erlenmeyer flask. Moreover, the amount of HPC (dosage) and the concentration of the metals and the prepared solution pH were based on the values provided by the CCD design.

In total, 20 experimental runs were carried out using the selected full-faced CCD design created with the statistical software Design Expert V11. The responses to which the effect of these factors was being studied are the removal capacity of HPC for Cd²⁺ (Y1) and Pb²⁺ (Y2). Based on the chosen full-faced CCD, a total number of 20 experimental runs were created using the statistical software Design Expert V11. The CCD design matrix showing each of the factors and their corresponding levels is presented in Table 1. The selected levels were based on the outcomes of the preliminary adsorption experiments conducted. The obtained responses were fitted to the polynomial expression described in Equation (2) below.

$$y = \beta_0 + \sum_{i=1}^k \beta_i x_i + \sum_{i=1}^k \beta_{ii} x_i^2 + \sum_{i=1}^{k-1} \sum_{j=2}^k \beta_{ij} x_i x_j + \varepsilon \quad (2)$$

where, β_0 , β_i , β_{ii} , β_{ij} , represent the constant, linear, square and interaction coefficients, respectively, while X_i , and X_j denote the factors considered, and y is the removal capacity of HPCs for each of the contaminants. Analysis of variance tests were performed to evaluate the adequacy of the fitted models and the significance of each of the factors on the studied responses.

Table 1. Central Composite Design for the adsorption experiment.

Factor	Coded Level	Values of Coded Levels		
		1	0	1
Initial Conc. (mg/L) (A)	X ₁	10	55	100
Adsorbent Dosage (g/L) (B)	X ₂	1	3	5
pH (C)	X ₃	3	5	7

5. Results and Discussion

A series of hierarchical porous carbons with abundant mesopores and macropores were fabricated via the ice-templation approach. SEM and TEM images in Figure 1a,b depict an open foam-like structure with mesoporosity replicating the etched silica template. The nitrogen isotherms as in Figure 1c exhibit IV type characteristics, indicating that the HPCs possess mainly mesopores. Table 2 presents the textural characteristics of HPCs.

Clearly, HPCs exhibit a broad range of BET-specific surface area up to 1100 m²/g, pore volume up to 3 cm³/g, and controlled dominant average mesopore size.

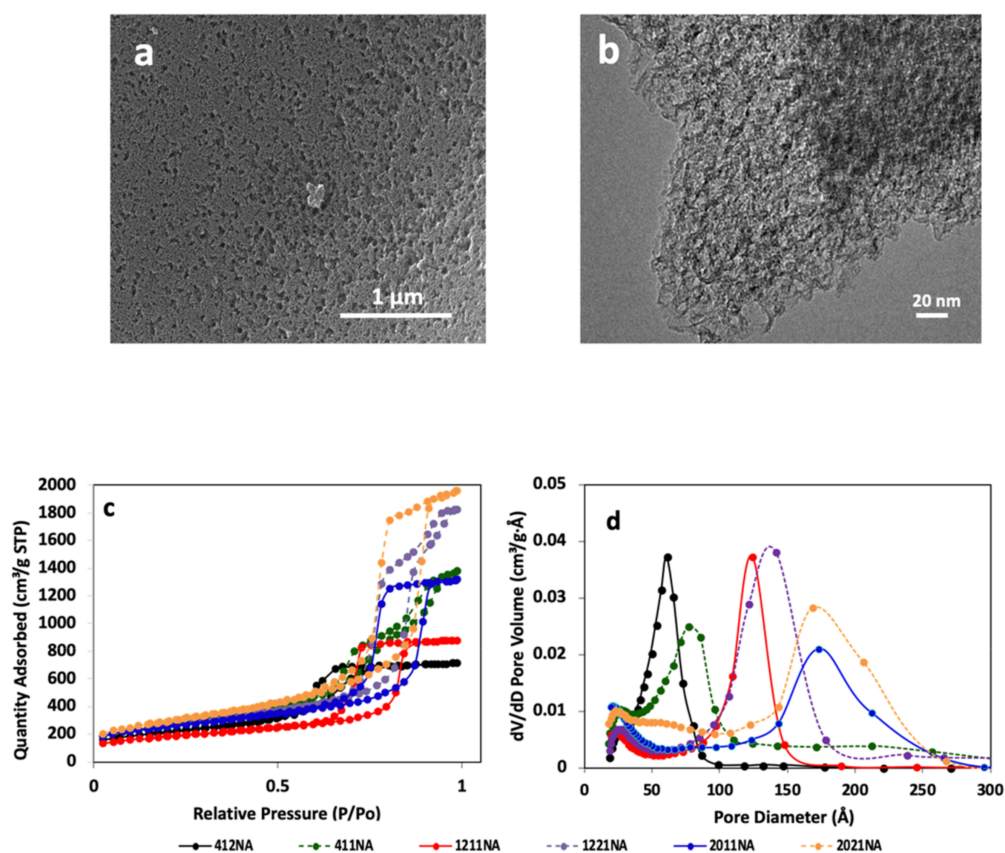


Figure 1. (a) Representative SEM image of HPC, (b) representative TEM image of HPC, (c) N₂ adsorption-desorption isotherms, and (d) pore size distributions of all the synthesized HPCs.

Table 2. BET-specific surface areas and pore volumes of the synthesized HPCs obtained via nitrogen adsorption at 77.3 K.

	BET Surface Area [m ² g ⁻¹]	t-Plot Micropore [m ² g ⁻¹]	Mesopore Surface Area [m ² g ⁻¹]	Total Pore Volume [cm ³ g ⁻¹]	Mesopore Volume [cm ³ g ⁻¹]	Micropore Volume [cm ³ g ⁻¹]	Average Mesopore Size [nm]
HPC412	747	100	647	1.1	1.1	0.05	6
HPC411	947	59	888	2.2	2.2	0.02	7
HPC1211	628	112	516	1.4	1.3	0.05	12
HPC1221	907	112	795	2.8	2.8	0.05	12
HPC2011	884	176	708	2	1.9	0.08	17
HPC2021	1037	72	965	3	2.9	0.03	17

The Barret-Joyner-Halenda (BJH) method was used to calculate the pore size and pore size distribution. The BJH of the HPCs exhibits narrow pore size distribution with a single dominant peak centered around a mesopore size that replicates the etched silica template size. For instance, the pore size distribution of HPC1211, as in Figure 1d, illustrates a dominant peak centered at around 12 nm, which resembles the hard template size [62].

Besides controlling the mesopore size, the pore volume was varied by controlling the silica/sucrose ratio during the synthesis process. Interestingly, the adopted approach allows for the synthesizing of different pore volumes while maintaining the average mesopore size of the HPC. For instance, while maintaining a similar average mesopore size, HPC1221 possesses a pore volume two times higher than HPC1211.

Raman spectra can be used to reveal information about the degree of graphitization. All HPCs show two main peaks corresponding to D and G bands, as in Figure 2. The D band, which is centered at around 1350 cm^{-1} , is related to the occurrence of structural deformity in the carbon structure, and the G band (which is centered at around 1590 cm^{-1}) is related to sp^2 atoms stretching.

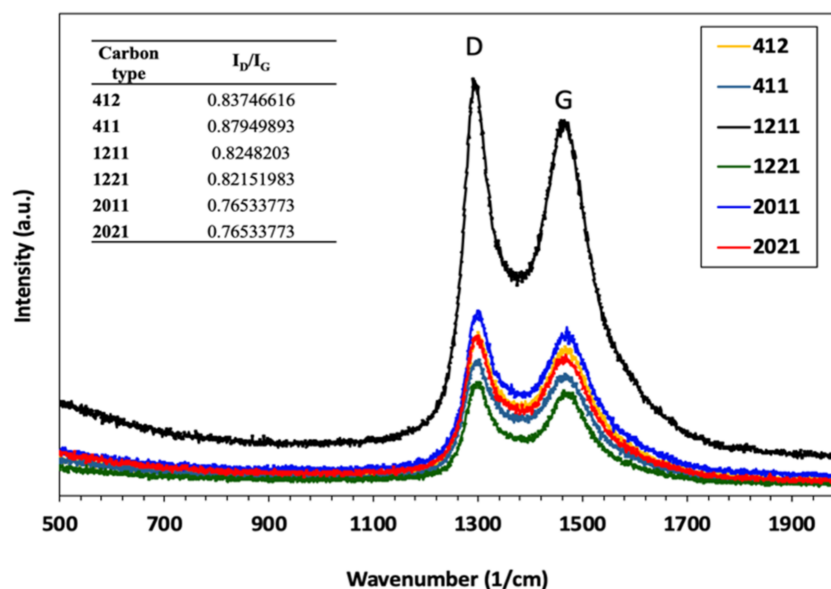


Figure 2. Raman spectra of HPCs.

The Raman intensity ratio (I_D/I_G) was used to estimate the degree of disorder for HPCs (see the inset of Figure 2) where a larger ratio indicates the large fraction of defects present in the HPCs. Doubling the pore volume for smaller mesopore HPCs (as in HPC412 and HPC411) leads to an increase in Raman ratio compared with larger mesopores (compare HPC2011 vs. HPC2021).

XPS analyses were used to characterize the chemical composition of the HPCs surface. The XPS spectra for nonetched HPC (HPC-SiO₂) and all the synthesized HPCs are shown in Figure 3. Post etching steps, the XPS spectra show a clear carbon C 1s peak, a smaller oxygen O 1s peak, and a disappeared silicon peak. Thus, the results indicate that all the hard template silica particles were successfully etched during the etching step.

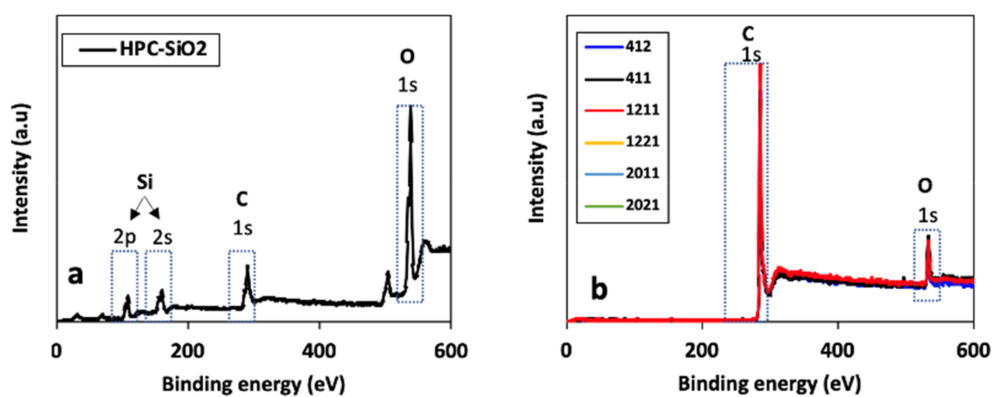


Figure 3. XPS survey scans for (a) HPC-SiO₂ prior to silica etching and (b) all HPCs.

5.1. Heavy Metal Removal Results

Results from adsorption time variation during Cd^{2+} and Pb^{2+} removal in both the single and binary solute systems by the HPC samples are presented in Figure 4.

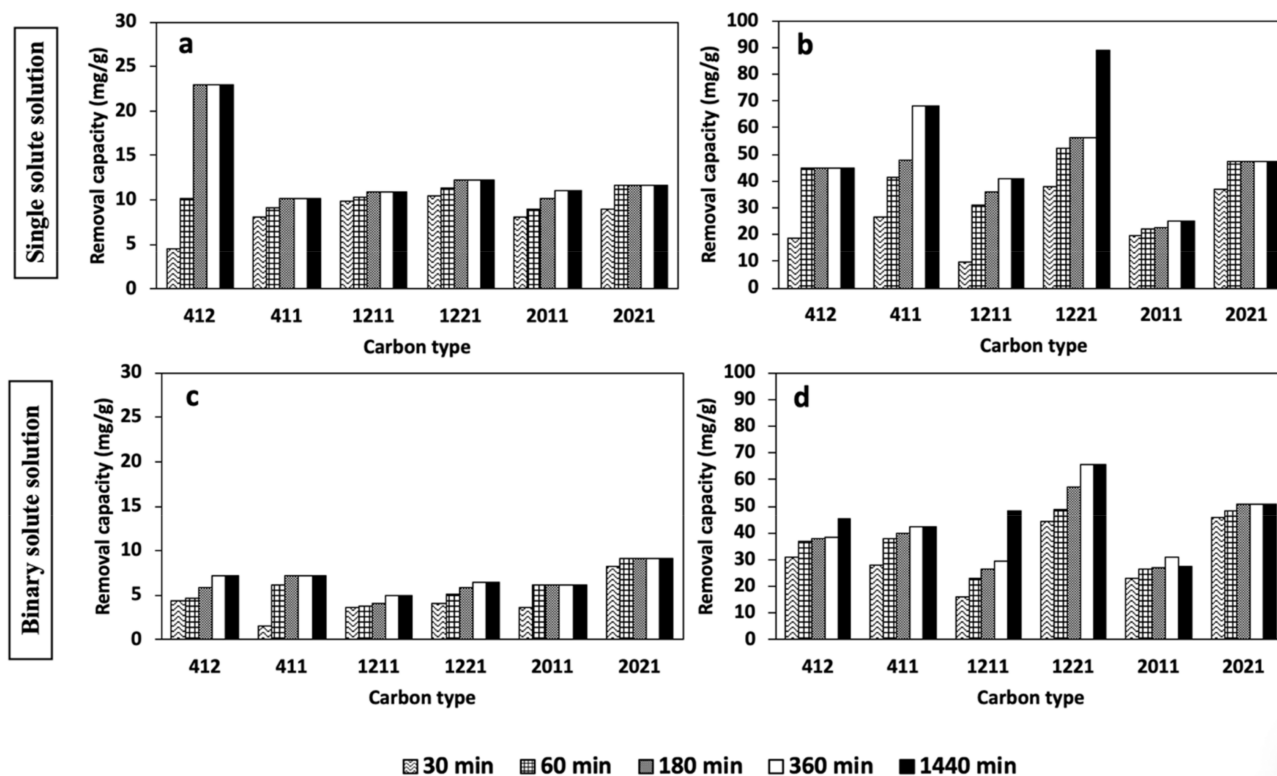


Figure 4. Removal time study of single (a,b) and binary (c,d) solute systems for the removal of Pb^{2+} (b,d) and Cd^{2+} (a,c).

Figure 4a presents the effect of adsorption time on Cd^{2+} removal by all the HPC samples in the single solute system. As illustrated, all the HPC samples presented a progressive increase in Cd^{2+} uptake over the entire period investigated, with an appreciable adsorbed amount of up to 22 mg/g. For all the HPC samples, HPC412 offered the highest uptake amount for Cd^{2+} , with an adsorbed amount of 22 mg/g after 180 min. On the other hand, the rest of the HPCs demonstrate a negligible increase in the metal ion uptake, even after a 24-h duration.

Figure 4b shows the adsorption of Pb^{2+} in the single solute system, where a progressive increase in uptake up to 89 mg/g in 24 h was observed. For all the HPCs, HPC1221 showed the highest uptake amount for Pb^{2+} , with an adsorbed amount of 38 mg/g at 30 min, which increased to 57 mg/g in 360 min and 89 mg/g after 24 h. Next, the HPC with the second-highest uptake for Pb^{2+} was HPC411, which presented a significant adsorbed amount of 68 mg/g after 360 min. Furthermore, the rest of the HPC samples provided an appreciable adsorbed amount of Pb^{2+} that was much better than that of Cd^{2+} . As a result, the HPCs had a higher affinity for Pb^{2+} than Cd^{2+} .

Similarly, the influence of increasing pore volume for the HPC sample pairs was also noted to be significant. As depicted, at 30 min of adsorption time, HPC2011 shows a Pb^{2+} uptake of 20 mg/g, while its counterpart with twice the pore volume (HPC2021) shows an enhanced uptake of 37 mg/g. In the same vein, HPC1211 and HPC412 show a low Pb^{2+} uptake of 9.6 mg/g and 18 mg/g, respectively, after 30 min, while their counterpart with twice the pore volume shows a slight increase in uptake of 38 mg/g and 27 mg/g, respectively, for the same time interval. A similar trend can also be seen after a 24 h mixing duration.

The results of Cd^{2+} and Pb^{2+} adsorption from the binary solute system shown in Figure 4c,d, indicates the occurrence of competition for HPCs' adsorption surface sites.

Furthermore, both the removal capacity (mg/g) and the removal rate (mg/g/min) are two important parameters that determine the performance of adsorbent material during the removal process [63]. While the removal capacity can be calculated by dividing the metal ions removed (mg) by the amount of the adsorbent material in (g), the removal rate, which is related to the kinetic of the removal process, can be calculated by dividing the metal ions' capacity (mg/g) by the duration of the removal experiment (min). Combining both parameters in a single plot can reveal and provide valuable information about the performance and allow one to optimize the removal process. Thus, in this work, a comparison between the performance of HPCs is presented by plotting the removal capacity (x -axis) against their removal rate (y -axis). Furthermore, an enhanced removal performance is manifested by the upper right shift in the diagram, where the adsorbent demonstrates a high removal capacity and rate. Additionally, optimization of the adsorption results of the HPCs can be achieved by multiplying the removal capacity by the removal rate.

Figure 5 illustrates a correlation between the removal capacity and removal rate of HPCs in Pb^{2+} removal experiments. For a specific mesopore size, doubling the pore volume for all the HPCs leads to a higher metal capacity and removal rate. However, such enhanced performance occurs to a different extent across the HPCs. A larger mesopore size can demonstrate better performance as a result of increasing the pore volume. This can be noticed by the upright shift of the plots.

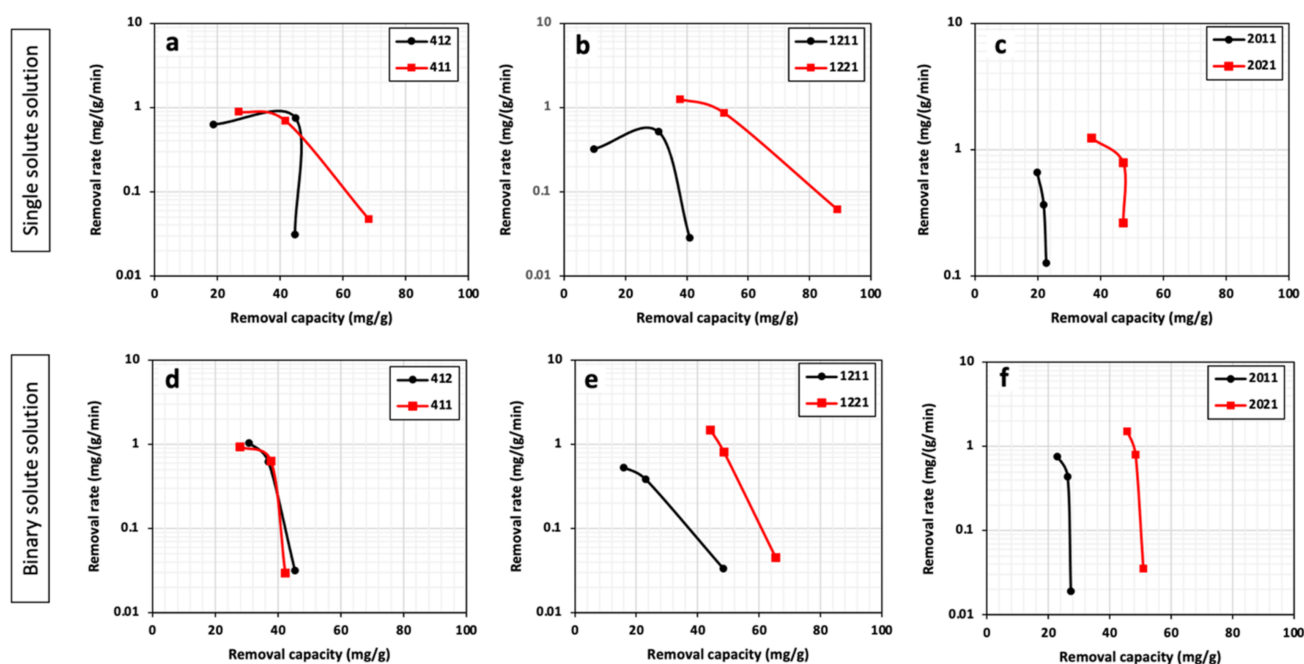


Figure 5. Removal rate vs. removal capacity of Pb^{2+} in single (a–c) and binary (d–f) solute systems for all HPCs.

By comparing the performance of a series of HPCs in binary and single solutions, generally, the removal capacity dropped (by different percentages) in the case of binary solutions. This can be ascribed to possible competition between the metals to occupy the available sites on the carbon material. Despite the drop in HPC removal capacity in a binary solution, the removal rate enhanced, especially at the beginning of the adsorption process. This was deduced from the upper shift of the curves for the binary solutions. For instance, while the highest removal rate of HPC1221 in a single solution is 1.26 mg/g/min, a binary solution demonstrates a higher value rate of 1.47 mg/g/min.

A similar removal capacity of HPC1221 for Pb removal can be seen in the case of Cd^{2+} removal. The removal of a single heavy metal solution leads to higher removal capability compared with a binary solution. However, the removal rates are higher in a single compared with a binary solution. For example, the cadmium removal rates for HPC1221 in binary and single solutions are 0.35 mg/g/min and 0.14 mg/g/min, respectively.

Interestingly, Figure 6 demonstrates that in both types of solutions (single and binary), increasing the pore volume for the studied mesopore size does not result in a significant effect in the removal of Cd^{2+} compared with when Pb^{2+} is used as a targeted heavy metal. Notably, HPC412 with around 50% less pore volume possesses a higher Cd^{2+} removal capability compared with HPC411.

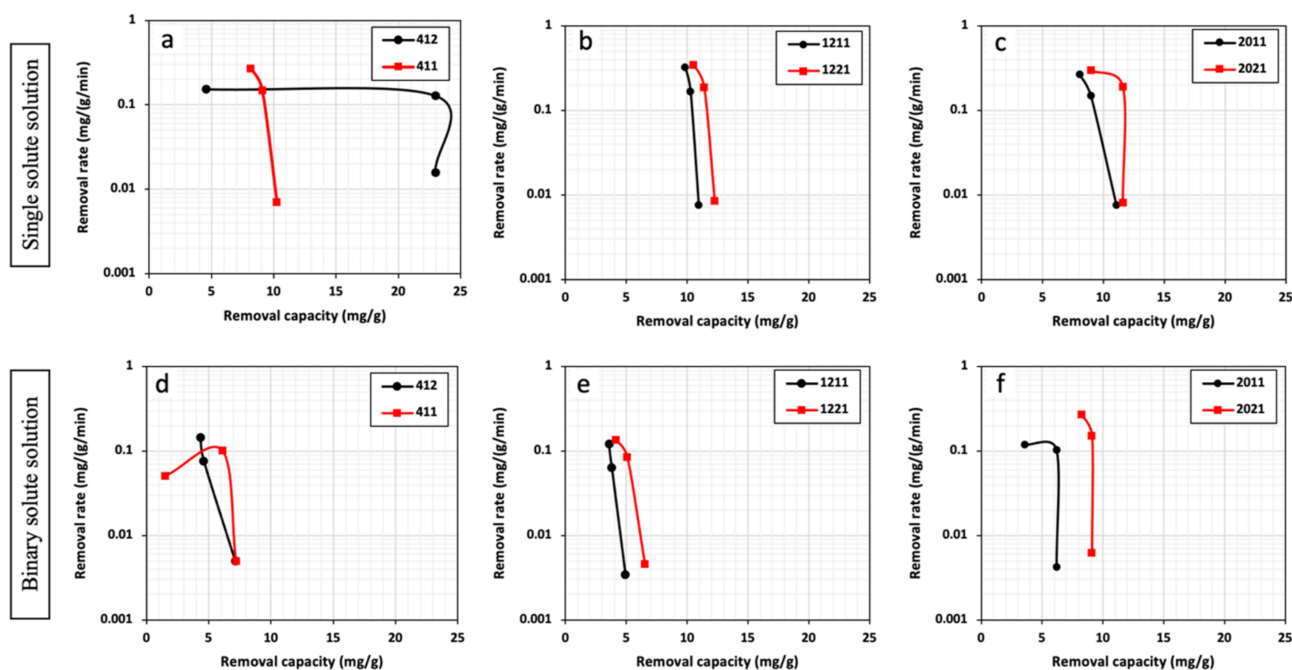


Figure 6. Removal rate vs. removal capacity of Cd^{2+} in single (a–c) and binary (d–f) solute systems for all HPCs.

Figure 7 shows the removal capacity of HPC1221 in a wide range of binary solution concentrations (10–200 ppm). HPC1221 removal capacity positively correlated with the solution concentration. At low concentration (i.e., 10 ppm), HPC1221 possesses comparable capacity for the removal of lead and cadmium. HPC1221 shows more affinity toward lead removal compared with cadmium. For instance, for the binary solution of (Pb–Cd) with 100 ppm concentration, the lead and cadmium removal capacity of HPC1221 is around 43 mg/g, 6.52 mg/g, respectively. This was further confirmed by comparing the HPC1221 capacity in a 100 ppm single solute solution. The HPC1221 still demonstrates a higher capacity for lead (89 mg/g) compared with cadmium (12.3 mg/g). Interestingly, in the case of a binary solution, the competition between different metals leads to a reduction in the HPC1221 uptake for lead and cadmium by 51% and 47%, respectively.

Figure 8 depicts the textural characteristics and the heavy metal removal capacity relationship for a series of HPCs. Figure 8a–c illustrates that the variation in textural characteristics leads to the different behavior of HPCs toward the removal of lead ions. Clearly, there is no general trend that correlates any of the textural characteristics and lead removal capacity of the HPCs. The results presented in Figure 8a–c indicate that a single textural characteristic of HPCs alone will not be a determinant factor in improving HPCs' performance. Lee and Park have found that heavy metal removal capacities do not positively correlate with surface area [64]. Accordingly, high surface area carbon could have a relatively lower adsorption capacity than that of lower surface area carbon. Additionally, although the majority of the pore volume of the activated carbon fibers (ACC) are

micropores, these micropores in the ACC are directly accessible for ions compared with ACs [51]. Reddy et al. compared the adsorption capacity of two activated carbons with similar surface areas [54]. They found that the activated carbon with a larger pore size demonstrated higher adsorption capacity, which was ascribed to easier diffusion of the targeted molecules into the pore. Similarly, Tamai et al. found that the adsorbent's pore size distribution is an important factor for enhancing the adsorption performance [55]. Therefore, optimizing the pore size, volume, and surface area in a porous carbon material is a key factor for enhancing the HPC's performance as an adsorbent material for lead removal.

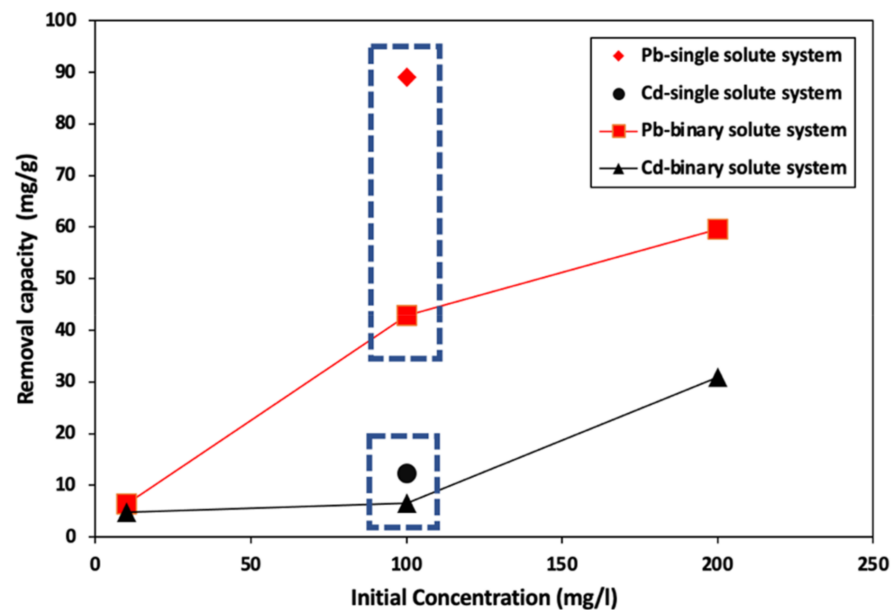


Figure 7. Removal capacity vs. initial concentration of HPC1221 in single and binary solute systems.

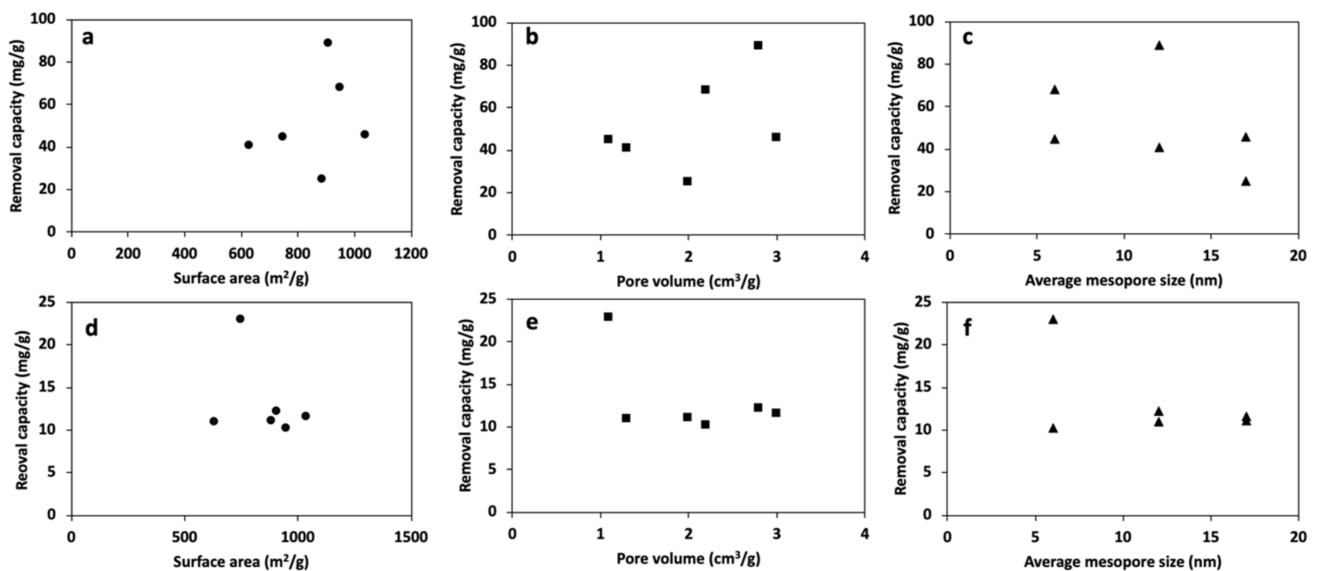


Figure 8. Removal capacity vs. (a,d) surface area, (b,e) pore volume, (c,f) average mesopore size of HPCs for Pb²⁺ (a–c) and Cd²⁺ (d–f) in a single solute system.

In Figure 8d–f, all HPCs show a lower capacity for cadmium compared with lead. Therefore, the lead has more driving force to be attracted to the HPCs' surfaces.

Notably, regardless of the wide variations in pore size, pore volume, and surface of the HPCs, all the HPCs demonstrate comparable cadmium removal. Thus, the textural characteristics of porous carbon have a negligible impact on the removal of cadmium ions. Hence, increasing the cadmium removal factors other than textural characteristics (i.e., surface chemistry) might result in a significant impact on enhancing the removal process.

5.2. Statistical Analysis and Response Surface Modelling

Since HPC1221 presented the best combination of removal capacity and removal rate for Cd^{2+} and Pb^{2+} , it was utilized for the subsequent experiments and statistical analysis. Table S1 presents the results of the CCD design matrix, showing the factor combinations and the corresponding actual experimental response and predicted response based on the fitted model. While employing the statistical design expert software, the actual experimental responses (Cd^{2+} and Pb^{2+} adsorbed amount) were fitted to a polynomial expression based on the coded values (A—initial Concentration, B—adsorbent dosage and C—pH), as shown in Equations (3) and (4).

Evaluation of the normality of the responses was carried out through the standard probability plots of the residuals displayed in Figure 9a,b. As illustrated, the experimental responses were approximately normally distributed based on these plots depicting a nearly straight line. In Figure 9c,d, the plots of predicted values (based on a fitted model) vs. the actual response values for Cd^{2+} and Pb^{2+} are provided. These plots indicate the existence of a good correlation between the actual and predicted response data.

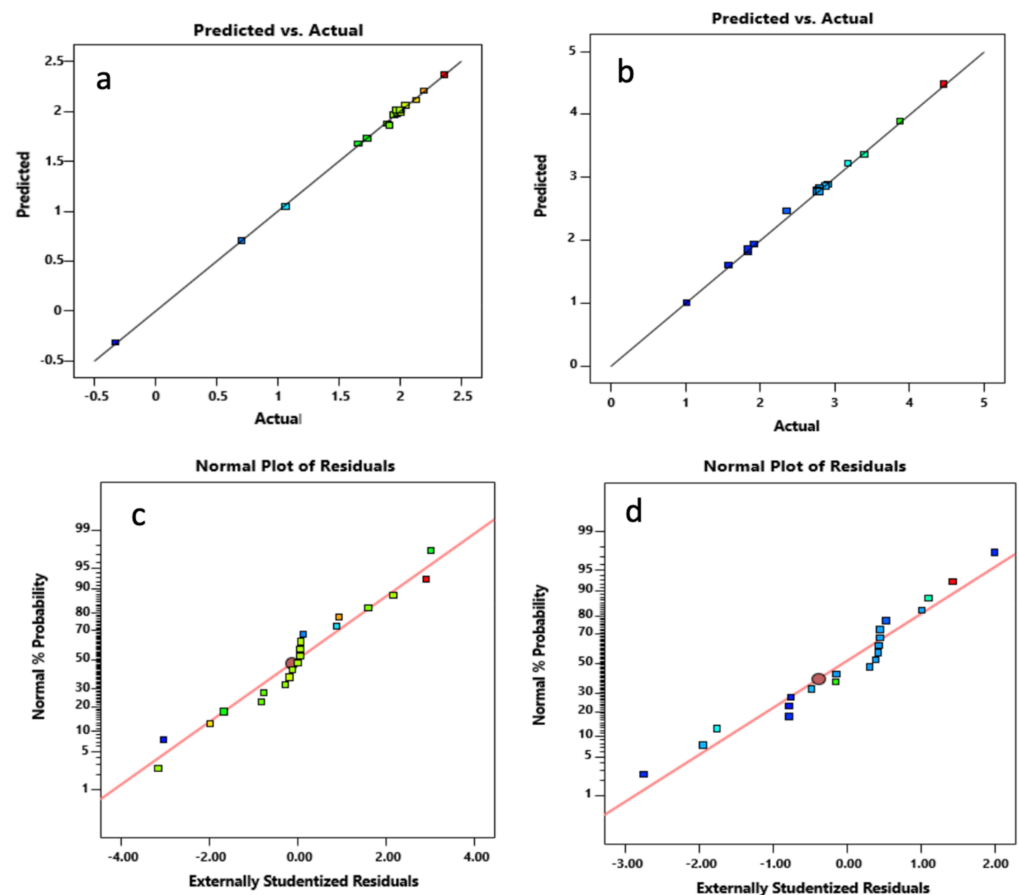


Figure 9. (a,b) Normal probability plots of the residuals and (c,d) plots of actual vs. predicted values of the responses.

The validity of the fitted models and the significance of the factors were evaluated through the Analysis of Variance Test (ANOVA). Parameters from the ANOVA test that include probability value (p -value), lack fit test value, correlation coefficient (R^2), adjusted R^2 , and predicted R^2 were used in validating the statistical relevance and adequacy of the fitted models.

Fitted Models in Terms of Coded Factors

$$\text{Ln}(\text{Cd}^{2+}) = 2.01 + 0.418 \times A + 0.174 \times B + 0.064 \times C + -0.094 \times AB + -0.317 \times AC - 0.083 \times BC + 0.550 \times A^2 + 0.0218 \times B^2 + 0.038 \times C^2 + 0.156 \times ABC + 0.374 \times A^2C + 0.153 \times AB^2 \quad (3)$$

$$\text{Ln}(\text{Pb}^{2+}) = 2.767 + 0.804 \times A + 0.450 \times B - 0.016 \times C + 0.206 \times AB - 0.023 \times AC - 0.035 \times BC - 0.361 \times A^2 + 0.137 \times B^2 + 0.043 \times C^2 + 0.188 \times ABC + 0.17839 \times A^2C + 0.136 \times AB^2 \quad (4)$$

Tables S2 and S3 show the results of the ANOVA test of factor significance. The significance level of each of the factors and their interaction were assessed based on the corresponding p -values at a 95% confidence interval. p -value > 0.05 signifies the statistical insignificance of the factor to the response, while p -values < 0.05 indicate the significance of the parameter to the response [65]. As illustrated for the two responses, all the individual factors, A—Initial concentration and B—adsorbent dosage and C—pH, were found to be statistically significant (p -values < 0.05). An exception to this was factor C-pH in the case of Pb^{2+} , which was insignificant as its p -value > 0.05 . This signifies that for the prepared HPC1221 adsorbent, pH variation has no impact on its uptake of Pb^{2+} .

The p -values for the models were also less than 0.05 (p -value < 0.0001), which signifies their statistical significance. The obtained R^2 and adjusted R^2 values for all the models (Table 3) were close to unity (1). In addition, a good agreement between the adjusted R^2 and the predicted R^2 for all the models was also observed (this occurs when their difference is less than 0.2). There was an adequate precision value, a measure of signal to noise ratio, with a value of 4 indicating an adequate signal for a model with a good predictive capability. The adequate precision values for all the models were greater than 4. In summary, all the above analyses were able to substantiate the adequacy of the models and indicate their good predictive capability for the experiment responses.

Table 3. Fit statistics of the fitted models.

	Response Transformation	Std Devember	Mean	C.V%	R^2	Adj. R^2	Predicted R^2	Adequate Precision
Cd^{2+}	Natural Log	0.0336	1.76	1.90	0.9989	0.9971	0.8721	24.0034
Pb^{2+}	Natural Log	0.0525	2.68	1.96	0.9983	0.9955	0.7482	17.0026

6. Effect of the Factors on the Removal of Cd^{2+} and Pb^{2+}

Figure 10 depicts the simultaneous effect of the factors' AB and AC interactions on the adsorbed amount of Cd^{2+} and Pb^{2+} . In Figure 10a,b, an increased uptake of Cd^{2+} can be observed as A and B were increased simultaneously, followed by a slight decrease in uptake, which is noted after the optimum condition was achieved. The optimum conditions of the two factors were found to lie around higher values of A (60–90 mg/L) and B (4–5 g/L). In the case of factor C, its increase led to a significant Cd^{2+} uptake as factor B was increased simultaneously. The optimum range for factor B, as shown in the figure, was found to be around pH 6–7.

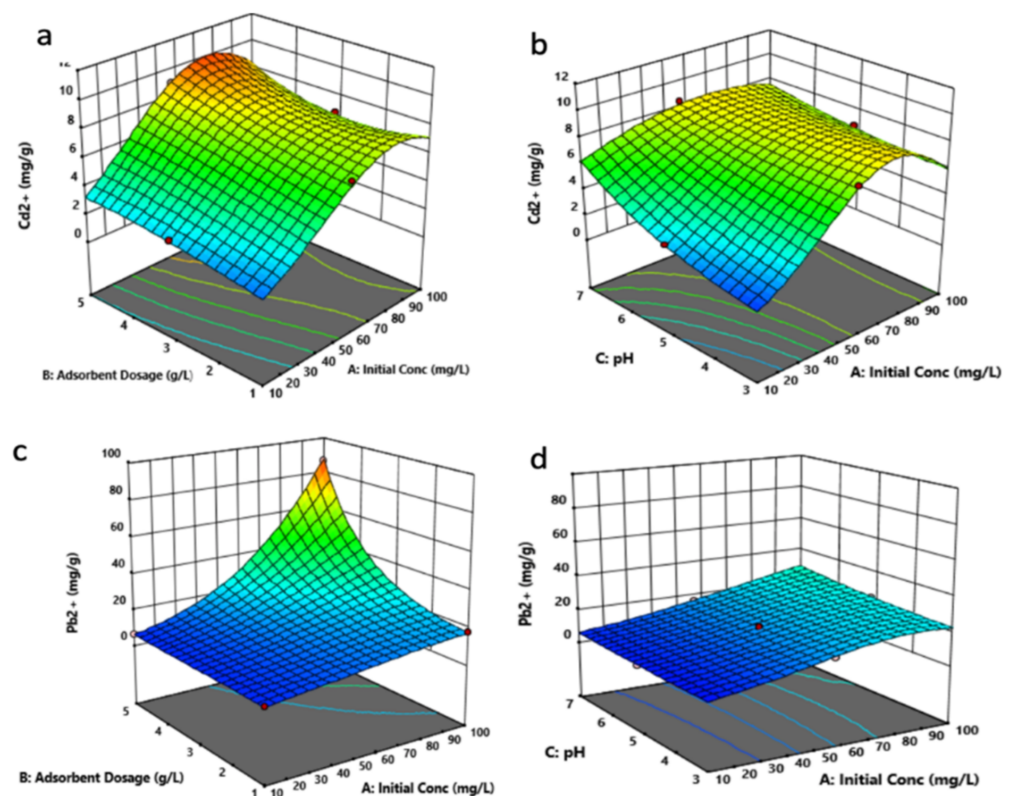


Figure 10. Simultaneous effect of the factors on Cd^{2+} (a,b) and Pb^{2+} (c,d) removal by HPC1221. Factor A: initial concentration, factor B: adsorbent dosage, and factor C: pH.

As for the influence of AB and BC interactions on Pb^{2+} removal shown in Figure 10c,d, an enhanced Pb^{2+} uptake was noted at higher values of A and B, while at lower values of these factors, a lower Pb^{2+} uptake was observed. As for factor C, its increase did not present any profound impact on Pb^{2+} uptake, as shown in Figure 10. This suggests that, irrespective of the pH values, the uptake amount of Pb^{2+} is shown to be dependent on the concentration and the adsorbent dosage. The optimum conditions for the factors of Pb^{2+} uptake were found to be at high values of A (90–100 mg/L) and B (5 mg/L). Based on the chemical speciation of cadmium and lead, it is averred that the major species of the two metals that will dominate at the pH range investigated are the ionic Cd^{2+} and Pb^{2+} [66–68]. Formation of the hydroxide species of the metals can occur at pH 6–7. However, it should be noted that these species are in the early stage of formation, and their concentration will be quite low compared with their ionic counterparts. Hence, the higher adsorbed amount of the two metals noted at around pH 7 in this study is likely because of the combined adsorption and precipitation process.

Based on these findings, it can be explained that the increase in factor A and B values, which led to the high uptake of Cd^{2+} and Pb^{2+} , can be ascribed to increased solute concentration and the availability of numerous surface binding sites in these conditions. Additionally, the high uptake noted at high C values (pH 6–7) for Cd^{2+} suggests the possible occurrence of precipitation via hydroxide formation by the metal along with adsorption, which resulted in an increased uptake rate by the HPC. On the other hand, irrespective of the pH values, the uptake amount of Pb^{2+} is shown to be dependent on the concentration and the adsorbent dosage.

7. Adsorption Isotherm

The adsorption behavior of Cd²⁺ and Pb²⁺ uptake by HPC1221 was evaluated through the modelling of the adsorption isotherm data. The obtained data were modelled using the conventional Langmuir and Freundlich isotherm models provided in Equations (5) and (6), respectively.

$$\frac{1}{q_e} = \frac{1}{q_m} + \frac{1}{K_L q_m} \frac{1}{C_e} \quad (5)$$

$$\ln q_e = \frac{1}{n} \ln C_e + \ln K_F \quad (6)$$

Here, q_e denotes the amount (mg/g) of Cd²⁺ and Pb²⁺ per unit mass of the AC at the equilibrium concentration C_e (mg/L). q_m is the maximum quantity of Cd²⁺ and Pb²⁺ per mass of adsorbent (mg/g). K_L is the Langmuir constant (L/mg) related to the adsorption energy. K_F is the Freundlich constant (mg/g)(L/mg)^{1/n}, and n is the Freundlich constant. The Langmuir isotherm model works on a theoretical assumption that describes the uptake of an adsorbate by the adsorbent according to a monolayer coverage mechanism over the homogenous surface sites without interaction between the adsorbed molecules, while the Freundlich isotherm model is an empirical relation that describes a multilayer adsorbate uptake onto the heterogeneous surface sites of the adsorbent with the occurrence of adsorbate molecules interaction.

The results of the fitted models plot are displayed in Figure 10, while the computed parameters are shown in Table S4. From the obtained R² values, Cd²⁺ adsorption is found to fit better with the Langmuir model when compared with the Freundlich model with R² values of 0.9844 and 0.9450, respectively. As for Pb²⁺, it was observed to be more suited to the Freundlich model because its R² value of 0.9930 was greater than that of the Langmuir model (R²: 0.8562). The computed Langmuir maximum adsorption capacity (HPC1221) of 10.02 mg/g for Cd²⁺ and 70.92 mg/g for Pb²⁺ were found to be close to the actual experimental maximum adsorption capacity value of 12.32 mg/g for Cd²⁺ and 89 mg/g for Pb²⁺. Table S5 shows a comparison of the surface properties and maximum adsorption capacities of different carbon adsorbents for Cd²⁺ and Pb²⁺ uptake. The reported adsorption capacities of the two metals were found to be better or comparable to those reported for pristine nonfunctionalized carbons. Notably, HPC1221 demonstrated a larger adsorption capacity for lead compared with other reported studies. On the other hand, HPC1221 possesses a moderate adsorption capacity for cadmium compared with other reported nonfunctionalized carbon materials.

Based on these findings, it was averred that Cd²⁺ uptake by HPC1221 was due to the monolayer physical adsorption process, while Pb²⁺ uptake was based on the multi-layer physisorption process. Monolayer adsorption implies that once the accessible surface binding sites of the adsorbent are occupied, solute adsorption will no longer take place. Thus, the lower uptake rate of Cd²⁺ reported in this study was likely due to the monolayer coverage, which subsequently impeded the aqueous Cd²⁺ uptake after the surface sites were exhausted. Furthermore, for Pb²⁺ adsorption, its suitable description by the multilayer isotherm model suggests that even after the surface sites were exhausted, the adsorbed Pb²⁺ interacted with the aqueous Pb²⁺ to aid their uptake in a multilayer fashion. This explanation is also in support of the higher adsorbed capacity noted for Pb²⁺ in this study. Hence, varying the textural characteristics of the HPCs is significant for Pb²⁺ removal compared with Cd²⁺.

The carbon synthesis procedure and the nature of the carbon precursors contribute significantly to the adsorption process [60]. Some studies employed different types of carbons with varied synthesis precursors and conditions, leaving many other variables such as the degree of the graphitization and the surface chemistry untested. Song et al. have investigated the adsorption properties of lead with four different carbon-based adsorbents and a wide range of surface areas (131.6–1014.4 m²/g) [69]. Although the rice-

husk-activated carbon had roughly 45 percent more surface area and micropore volume than saw-dust-activated carbon, both carbons had similar lead capacity (see Table S5). Furthermore, the tire-activated carbon with a $131.6 \text{ m}^2/\text{g}$ surface area and a $0.029 \text{ cm}^3/\text{g}$ micropore volume demonstrated a 62 percent higher lead capacity than acrylic-fiber-activated carbon with approximately six times the surface area and ten times the micropore volume. It is necessary to examine a wide range of mesopore sizes in order to understand the influence of mesopore size and volume. Table S5 shows that many of the reported studies investigated lower mesopore sizes (up to 5 nm), which may restrict the validity of their observations. Besides this, some of the reported studies in Table S5 showed a bimodal or trimodal (instead of unimodal) pore size distribution [70]. Notably, the lack of control over mesopore size can make it difficult to find and understand the correlations between the pore size and removal performance of the adsorbent materials. To better assess the role of the textural characteristics, it is important to evaluate the HPCs that were synthesized under the same conditions and using the same precursors. The employed synthesis approach in this work allows for the synthesis of a wide range of HPCs, and the fine-tuning of the carbon mesopore size and mesopore volume eliminates other effects that might arise from different synthesis conditions and utilization of different precursors. Thus, the findings in this study aided in the investigation of the relationships between textural characteristics and adsorbent materials' removal performance.

8. Conclusions

A series of finely tuned hierarchical porous carbons HPCs were synthesized and evaluated against the removal of lead and cadmium from an aqueous solution to determine the key design parameters for the adsorbent material. Interestingly, cadmium and lead responses vary in their dependence on the textural characteristics of HPCs. All the HPC samples presented a progressive increase in Cd^{2+} and Pb^{2+} uptake over the entire investigated period (24 h). This work demonstrated the effectiveness of optimizing the pore size, pore-volume, and surface area for enhancing HPC lead removal. All the HPCs with doubled pore volumes and similar dominant mesopore sizes resulted in enhanced lead uptakes (up to 300%). On the other hand, variations in the textural characteristics of HPCs have a negligible impact on the removal of cadmium. Factors other than textural characteristics (i.e., surface chemistry) might be significant in enhancing the removal performance of the adsorbents. Notably, all the HPCs demonstrated high affinities toward lead removal compared with cadmium. Hence, all the HPCs showed a lower removal capacity toward cadmium compared with lead. HPC1221 showed the maximum Cd^{2+} and Pb^{2+} adsorption capacity of 12.32 and 89 mg/g, respectively. Hence, the results suggested that HPC1221 possessed an optimum combination of textural characteristics (with 17 nm mesopore size, $2.8 \text{ cm}^3/\text{g}$ pore volume, and $907 \text{ m}^2/\text{g}$ surface area) of HPC as an adsorbent material for lead and cadmium removal. In a binary solution, the competition between different metals lowered the HPC1221 uptake of lead and cadmium by 51% and 47%, respectively. Notably, the highest removal rates of HPC1221 are higher in the case of the binary solution (Cd^{2+} 0.35, Pb^{2+} 1.47 mg/g/min) compared with the single solution (Cd^{2+} 0.14, Pb^{2+} 1.26 mg/g/min). In conclusion, defining key material parameters and designing an intelligent carbon porous structure can pave the way for high performing adsorbents for heavy metal removal.

Supplementary Materials: The following are available online at <https://www.mdpi.com/article/10.3390/su13115790/s1>. Table S1: CCD matrix of the experiment showing the factor combination and the responses. Table S2: ANOVA result for Cd^{2+} adsorption. Table S3: ANOVA result for Pb^{2+} adsorption., Figure S1: Figure 1. Langmuir and Freundlich isotherm plot for Cd^{2+} (a,b), and Pb^{2+} (c,d) adsorption, Table S4: Isotherm parameters, Table S5: Comparison of adsorption capacities of some non-functionalized carbon adsorbents for Cd^{2+} and Pb^{2+} .

Funding: This research was funded by the Deanship of Scientific Research, King Fahd University of Petroleum and Minerals, project number SR-181009.

Institutional Review Board Statement: Not applicable.

Informed Consent Statement: Not applicable.

Data Availability Statement: Not applicable.

Acknowledgments: Turki N. Baroud acknowledges the Deanship of Scientific Research, KFUPM, for supporting this work under the project# SR-181009. The author thanks C. Basheer for his help and useful discussions regarding the Atomic Absorption Spectrometer (AAS) measurements. Additionally, the author also thanks M. Dauda for his help and useful discussions regarding statistical analysis, response surface modelling, and adsorption isotherms. This work made use of Materials for Energy and Water laboratory, Mechanical engineering department, KFUPM.

Conflicts of Interest: The author declares no conflict of interest.

References

1. Subramani, A.; Jacangelo, J.G. Emerging desalination technologies for water treatment: A critical review. *Water Res.* **2015**, *75*, 164–187. [[CrossRef](#)] [[PubMed](#)]
2. Xu, P.; Drewes, J.E.; Heil, D.; Wang, G. Treatment of brackish produced water using carbon aerogel-based capacitive deionization technology. *Water Res.* **2008**, *42*, 2605–2617. [[CrossRef](#)] [[PubMed](#)]
3. Srivastava, N.; Majumder, C. Novel biofiltration methods for the treatment of heavy metals from industrial wastewater. *J. Hazard. Mater.* **2008**, *151*, 1–8. [[CrossRef](#)] [[PubMed](#)]
4. Kannan, N.; Rengasamy, G. Comparison of Cadmium Ion Adsorption on Various ACTIVATED CARBONS. *Water Air Soil Pollut.* **2005**, *163*, 185–201. [[CrossRef](#)]
5. Sharma, H.; Rawal, N.; Mathew, B.B. The Characteristics, Toxicity and Effects of Cadmium. *Int. J. Nanotechnol. Nanosci.* **2015**, *3*, 1–9.
6. Jellali, S.; Azzaz, A.A.; Jeguirim, M.; Hamdi, H.; Mlayah, A. Use of Lignite as a Low-Cost Material for Cadmium and Copper Removal from Aqueous Solutions: Assessment of Adsorption Characteristics and Exploration of Involved Mechanisms. *Water* **2021**, *13*, 164. [[CrossRef](#)]
7. Fattahi, M.; Ezzatzadeh, E.; Jalilian, R.; Taheri, A. Micro solid phase extraction of cadmium and lead on a new ion-imprinted hierarchical mesoporous polymer via dual-template method in river water and fish muscles: Optimization by experimental design. *J. Hazard. Mater.* **2021**, *403*, 123716. [[CrossRef](#)]
8. Peer, F.E.; Bahramifar, N.; Younesi, H. Removal of Cd (II), Pb (II) and Cu (II) ions from aqueous solution by polyamidoamine dendrimer grafted magnetic graphene oxide nanosheets. *J. Taiwan Inst. Chem. Eng.* **2018**, *87*, 225–240. [[CrossRef](#)]
9. Zargoosh, K.; Abedini, H.; Abdolmaleki, A.; Molavian, M.R. Effective Removal of Heavy Metal Ions from Industrial Wastes Using Thiosalicylhydrazide-Modified Magnetic Nanoparticles. *Ind. Eng. Chem. Res.* **2013**, *52*, 14944–14954. [[CrossRef](#)]
10. Wu, J.; Wang, T.; Wang, J.; Zhang, Y.; Pan, W.-P. A novel modified method for the efficient removal of Pb and Cd from wastewater by biochar: Enhanced the ion exchange and precipitation capacity. *Sci. Total Environ.* **2021**, *754*, 142150. [[CrossRef](#)]
11. Abbas, A.; Al-Amer, A.M.; Laoui, T.; Al-Marri, M.J.; Nasser, M.S.; Khraisheh, M.; Atieh, M.A. Heavy metal removal from aqueous solution by advanced carbon nanotubes: Critical review of adsorption applications. *Sep. Purif. Technol.* **2016**, *157*, 141–161. [[CrossRef](#)]
12. Sajid, M.; Nazal, M.K.; Baig, N.; Osman, A.M. Removal of heavy metals and organic pollutants from water using dendritic polymers based adsorbents: A critical review. *Sep. Purif. Technol.* **2018**, *191*, 400–423. [[CrossRef](#)]
13. Clark, T.; Stephenson, T.; Pearce, P. Phosphorus removal by chemical precipitation in a biological aerated filter. *Water Res.* **1997**, *31*, 2557–2563. [[CrossRef](#)]
14. Mbamba, C.K.; Batstone, D.J.; Flores-Alsina, X.; Tait, S. A generalised chemical precipitation modelling approach in wastewater treatment applied to calcite. *Water Res.* **2015**, *68*, 342–353. [[CrossRef](#)]
15. Wang, X.; Xia, S.; Chen, L.; Zhao, J.; Renault, N.; Chovelon, J. Nutrients removal from municipal wastewater by chemical precipitation in a moving bed biofilm reactor. *Process. Biochem.* **2006**, *41*, 824–828. [[CrossRef](#)]
16. Fu, F.; Xie, L.; Tang, B.; Wang, Q.; Jiang, S. Application of a novel strategy—Advanced Fenton-chemical precipitation to the treatment of strong stability chelated heavy metal containing wastewater. *Chem. Eng. J.* **2012**, *189–190*, 283–287. [[CrossRef](#)]
17. Hosseini, S.; Amini, S.; Khodabakhshi, A.; Bagheripour, E.; Van der Bruggen, B. Activated carbon nanoparticles entrapped mixed matrix polyethersulfone based nanofiltration membrane for sulfate and copper removal from water. *J. Taiwan Inst. Chem. Eng.* **2018**, *82*, 169–178. [[CrossRef](#)]
18. Abdi, G.; Alizadeh, A.; Zinadini, S.; Moradi, G. Removal of dye and heavy metal ion using a novel synthetic polyethersulfone nanofiltration membrane modified by magnetic graphene oxide/metformin hybrid. *J. Membr. Sci.* **2018**, *552*, 326–335. [[CrossRef](#)]
19. Tran, T.-K.; Chiu, K.-F.; Lin, C.-Y.; Leu, H.-J. Electrochemical treatment of wastewater: Selectivity of the heavy metals removal process. *Int. J. Hydrog. Energy* **2017**, *42*, 27741–27748. [[CrossRef](#)]

20. Al Hamouz, O.C.S.; Estatie, M.; Saleh, T.A. Removal of cadmium ions from wastewater by dithiocarbamate functionalized pyrrole based terpolymers. *Sep. Purif. Technol.* **2017**, *177*, 101–109. [[CrossRef](#)]
21. Li, Q.; Yu, J.; Zhou, F.; Jiang, X. Synthesis and characterization of dithiocarbamate carbon nanotubes for the removal of heavy metal ions from aqueous solutions. *Colloids Surf. A Physicochem. Eng. Asp.* **2015**, *482*, 306–314. [[CrossRef](#)]
22. Tofighy, M.A.; Mohammadi, T. Adsorption of divalent heavy metal ions from water using carbon nanotube sheets. *J. Hazard. Mater.* **2011**, *185*, 140–147. [[CrossRef](#)] [[PubMed](#)]
23. Taamneh, Y.; Sharadqah, S. The removal of heavy metals from aqueous solution using natural Jordanian zeolite. *Appl. Water Sci.* **2017**, *7*, 2021–2028. [[CrossRef](#)]
24. Erdem, E.; Karapinar, N.; Donat, R. The removal of heavy metal cations by natural zeolites. *J. Colloid Interface Sci.* **2004**, *280*, 309–314. [[CrossRef](#)]
25. Zanin, E.; Scapinello, J.; de Oliveira, M.; Rambo, C.L.; Franscescon, F.; Freitas, L.; de Mello, J.M.M.; Fiori, M.A.; Oliveira, J.; Magro, J.D. Adsorption of heavy metals from wastewater graphic industry using clinoptilolite zeolite as adsorbent. *Process. Saf. Environ. Prot.* **2017**, *105*, 194–200. [[CrossRef](#)]
26. Cervera, M.L.; Arnal, M.C.; De La Guardia, M. Removal of heavy metals by using adsorption on alumina or chitosan. *Anal. Bioanal. Chem.* **2003**, *375*, 820–825. [[CrossRef](#)]
27. Kim, Y.; Kim, C.; Choi, I.; Rengaraj, S.; Yi, J. Arsenic Removal Using Mesoporous Alumina Prepared via a Templating Method. *Environ. Sci. Technol.* **2003**, *38*, 924–931. [[CrossRef](#)]
28. Gao, W.; Fatehi, P. Fly ash based adsorbent for treating bleaching effluent of kraft pulping process. *Sep. Purif. Technol.* **2018**, *195*, 60–69. [[CrossRef](#)]
29. Cetin, S.; Pehlivan, E. The use of fly ash as a low cost, environmentally friendly alternative to activated carbon for the removal of heavy metals from aqueous solutions. *Colloids Surf. A Physicochem. Eng. Asp.* **2007**, *298*, 83–87. [[CrossRef](#)]
30. Hua, M.; Zhang, S.; Pan, B.; Zhang, W.; Lv, L.; Zhang, Q. Heavy metal removal from water/wastewater by nanosized metal oxides: A review. *J. Hazard. Mater.* **2012**, *211–212*, 317–331. [[CrossRef](#)]
31. Pelalak, R.; Heidari, Z.; Khatami, S.M.; Kurniawan, T.A.; Marjani, A.; Shirazian, S. Oak wood ash/GO/Fe₃O₄ adsorption efficiencies for cadmium and lead removal from aqueous solution: Kinetics, equilibrium and thermodynamic evaluation. *Arab. J. Chem.* **2021**, *14*, 102991. [[CrossRef](#)]
32. Fu, F.; Wang, Q. Removal of heavy metal ions from wastewaters: A review. *J. Environ. Manag.* **2011**, *92*, 407–418. [[CrossRef](#)]
33. Babel, S.; Kurniawan, T.A. Low-cost adsorbents for heavy metals uptake from contaminated water: A review. *J. Hazard. Mater.* **2003**, *97*, 219–243. [[CrossRef](#)]
34. Gupta, V.K.; Srivastava, S.K.; Mohan, D.; Sharma, S. Original Contribution Design Parameters for Fixed Bed Reactors of Activated Carbon Developed From Fertilizer Waste for the Removal of S O M E Heavy Metal Ions. *Pergamon* **1998**, *17*, 517–522.
35. Karnib, M.; Kabbani, A.; Holail, H.; Olama, Z. Heavy Metals Removal Using Activated Carbon, Silica and Silica Activated Carbon Composite. *Energy Procedia* **2014**, *50*, 113–120. [[CrossRef](#)]
36. Amuda, O.; Giwa, A.; Bello, I. Removal of heavy metal from industrial wastewater using modified activated coconut shell carbon. *Biochem. Eng. J.* **2007**, *36*, 174–181. [[CrossRef](#)]
37. Kobya, M.; Demirbas, E.; Senturk, E.; Ince, M. Adsorption of heavy metal ions from aqueous solutions by activated carbon prepared from apricot stone. *Bioresour. Technol.* **2005**, *96*, 1518–1521. [[CrossRef](#)]
38. Corapcioglu, M.; Huang, C. The adsorption of heavy metals onto hydrous activated carbon. *Water Res.* **1987**, *21*, 1031–1044. [[CrossRef](#)]
39. Kadirvelu, K.; Thamaraiselvi, K.; Namasivayam, C. Removal of heavy metals from industrial wastewaters by adsorption onto activated carbon prepared from an agricultural solid waste. *Bioresour. Technol.* **2001**, *76*, 63–65. [[CrossRef](#)]
40. Hydari, S.; Shariffard, H.; Nabavinia, M.; Parvizi, M.R. A comparative investigation on removal performances of commercial activated carbon, chitosan biosorbent and chitosan/activated carbon composite for cadmium. *Chem. Eng. J.* **2012**, *193–194*, 276–282. [[CrossRef](#)]
41. Modin, H.; Persson, K.M.; Andersson, A.; van Praagh, M. Removal of metals from landfill leachate by sorption to activated carbon, bone meal and iron fines. *J. Hazard. Mater.* **2011**, *189*, 749–754. [[CrossRef](#)] [[PubMed](#)]
42. Ihsanullah. Carbon nanotube membranes for water purification: Developments, challenges, and prospects for the future. *Sep. Purif. Technol.* **2019**, *209*, 307–337. [[CrossRef](#)]
43. Jawed, A.; Saxena, V.; Pandey, L.M. Engineered nanomaterials and their surface functionalization for the removal of heavy metals: A review. *J. Water Process. Eng.* **2020**, *33*, 101009. [[CrossRef](#)]
44. Schwieger, C. Electrostatic and Non-Electrostatic Interactions of Positively Charged Polypeptides with Negatively Charged Lipid Membranes. Ph.D. Thesis, Martin-Luther-University Halle-Wittenberg, Halle, Germany, 2008.
45. Ouyang, X.-K.; Yang, L.-P.; Wen, Z.-S. Adsorption of Pb(II) from Solution using Peanut Shell as Biosorbent in the Presence of Amino Acid and Sodium Chloride. *Bioresources* **2014**, *9*, 2446–2458. [[CrossRef](#)]
46. Hadi, P.; Barford, J.; McKay, G. Toxic Heavy Metal Capture Using a Novel Electronic Waste-Based Material—Mechanism, Modeling and Comparison. *Environ. Sci. Technol.* **2013**, *47*, 8248–8255. [[CrossRef](#)]
47. Sarkar, B.; Mandal, S.; Tsang, Y.F.; Kumar, P.; Kim, K.-H.; Ok, Y.S. Designer carbon nanotubes for contaminant removal in water and wastewater: A critical review. *Sci. Total Environ.* **2018**, *612*, 561–581. [[CrossRef](#)] [[PubMed](#)]

48. Yin, C.-Y.; Aroua, M.K.; Mohamed, K.; Daud, W. Review of modifications of activated carbon for enhancing contaminant uptakes from aqueous solutions. *Sep. Purif. Technol.* **2007**, *52*, 403–415. [[CrossRef](#)]
49. Zhi, Y.; Liu, J. Surface modification of activated carbon for enhanced adsorption of perfluoroalkyl acids from aqueous solutions. *Chemosphere* **2016**, *144*, 1224–1232. [[CrossRef](#)]
50. Song, X.; Liu, H.; Cheng, L.; Qu, Y. Surface modification of coconut-based activated carbon by liquid-phase oxidation and its effects on lead ion adsorption. *Desalination* **2010**, *255*, 78–83. [[CrossRef](#)]
51. Rangel-Mendez, J.; Sreat, M. Adsorption of cadmium by activated carbon cloth: Influence of surface oxidation and solution pH. *Water Res.* **2002**, *36*, 1244–1252. [[CrossRef](#)]
52. Ahn, C.K.; Park, D.; Woo, S.H.; Park, J.M. Removal of cationic heavy metal from aqueous solution by activated carbon impregnated with anionic surfactants. *J. Hazard. Mater.* **2009**, *164*, 1130–1136. [[CrossRef](#)] [[PubMed](#)]
53. Gupta, V.K.; Ganjali, M.; Nayak, A.; Bhushan, B.; Agarwal, S. Enhanced heavy metals removal and recovery by mesoporous adsorbent prepared from waste rubber tire. *Chem. Eng. J.* **2012**, *197*, 330–342. [[CrossRef](#)]
54. Reddy, K.S.K.; Al Shoaibi, A.; Srinivasakannan, C. A comparison of microstructure and adsorption characteristics of activated carbons by CO₂ and H₃PO₄ activation from date palm pits. *New Carbon Mater.* **2012**, *27*, 344–351. [[CrossRef](#)]
55. Tamai, H.; Yoshida, T.; Sasaki, M.; Yasuda, H. Dye adsorption on mesoporous activated carbon fiber obtained from pitch containing yttrium complex. *Carbon* **1999**, *37*, 983–989. [[CrossRef](#)]
56. Zhao, S.; Yan, T.; Wang, H.; Zhang, J.; Shi, L.; Zhang, D. Creating 3D Hierarchical Carbon Architectures with Micro-, Meso-, and Macropores via a Simple Self-Blowing Strategy for a Flow-through Deionization Capacitor. *ACS Appl. Mater. Interfaces* **2016**, *8*, 18027–18035. [[CrossRef](#)]
57. Zhu, S.; Li, J.; He, C.; Zhao, N.; Liu, E.; Shi, C.; Zhang, M. Soluble salt self-assembly-assisted synthesis of three-dimensional hierarchical porous carbon networks for supercapacitors. *J. Mater. Chem. A* **2015**, *3*, 22266–22273. [[CrossRef](#)]
58. Younas, M.; Baroud, T.N.; Gondal, M.; Dastageer, M.; Giannelis, E.P. Highly efficient, cost-effective counter electrodes for dye-sensitized solar cells (DSSCs) augmented by highly mesoporous carbons. *J. Power Sources* **2020**, *468*, 228359. [[CrossRef](#)]
59. Nanaki, S.G.; Spyrou, K.; Bekiari, C.; Veneti, P.; Baroud, T.N.; Karouta, N.; Grivas, I.; Papadopoulos, G.C.; Gournis, D.; Bikiaris, D.N. Hierarchical Porous Carbon—PLLA and PLGA Hybrid Nanoparticles for Intranasal Delivery of Galantamine for Alzheimer's Disease Therapy. *Pharmaceutics* **2020**, *12*, 227. [[CrossRef](#)]
60. Crini, G.; Lichtfouse, E.; Wilson, L.D.; Morin-Crini, N. Adsorption-oriented processes using conventional and non-conventional adsorbents for wastewater treatment. In *Green Adsorbents for Pollutant Removal*; Springer: Berlin/Heidelberg, Germany, 2018; Volume 18, pp. 23–71. [[CrossRef](#)]
61. Baroud, T.N.; Giannelis, E.P. High salt capacity and high removal rate capacitive deionization enabled by hierarchical porous carbons. *Carbon* **2018**, *139*, 614–625. [[CrossRef](#)]
62. Estevez, L.; Dua, R.; Bhandari, N.; Ramanujapuram, A.; Wang, P.; Giannelis, E.P. A facile approach for the synthesis of monolithic hierarchical porous carbons – high performance materials for amine based CO₂ capture and supercapacitor electrode. *Energy Environ. Sci.* **2013**, *6*, 1785–1790. [[CrossRef](#)]
63. Baroud, T.N.; Giannelis, E.P. Role of Mesopore Structure of Hierarchical Porous Carbons on the Electrosorption Performance of Capacitive Deionization Electrodes. *ACS Sustain. Chem. Eng.* **2019**, *7*, 7580–7596. [[CrossRef](#)]
64. Hadi, P.; Xu, M.; Ning, C.; Lin, C.S.K.; McKay, G. A critical review on preparation, characterization and utilization of sludge-derived activated carbons for wastewater treatment. *Chem. Eng. J.* **2015**, *260*, 895–906. [[CrossRef](#)]
65. Baylan, N.; Çehreli, S. Ionic liquids as bulk liquid membranes on levulinic acid removal: A design study. *J. Mol. Liq.* **2018**, *266*, 299–308. [[CrossRef](#)]
66. Wang, X.; Wang, L.; Wang, Y.; Tan, R.; Ke, X.; Zhou, X.; Geng, J.; Hou, H.; Zhou, M. Calcium Sulfate Hemihydrate Whiskers Obtained from Flue Gas Desulfurization Gypsum and Used for the Adsorption Removal of Lead. *Crystals* **2017**, *7*, 270. [[CrossRef](#)]
67. Powell, K.J.; Brown, P.L.; Byrne, R.H.; Gajda, T.; Hefter, G.; Leuz, A.-K.; Sjöberg, S.; Wanner, H. Chemical speciation of environmentally significant metals with inorganic ligands. Part 4: The Cd²⁺ + OH⁻, Cl⁻, CO₃²⁻, SO₄²⁻, and PO₄³⁻ systems (IUPAC Technical Report). *Pure Appl. Chem.* **2011**, *83*, 1163–1214. [[CrossRef](#)]
68. Powell, K.J.; Brown, P.L.; Byrne, R.H.; Gajda, T.; Hefter, G.; Leuz, A.K.; Sjöberg, S.; Wanner, H. Chemical speciation of environmentally significant metals with inorganic ligands. Part 3: The Pb²⁺ + OH⁻, Cl⁻, CO₃²⁻, SO₄²⁻, and PO₄³⁻ systems (IUPAC Technical Report). *Pure Appl. Chem.* **2009**, *81*, 2425–2476. [[CrossRef](#)]
69. Nieto-Márquez, A.; Pinedo-Flores, A.; Picasso, G.; Atanes, E.; Kou, R.S. Selective adsorption of Pb²⁺, Cr³⁺ and Cd²⁺ mixtures on activated carbons prepared from waste tires. *J. Environ. Chem. Eng.* **2017**, *5*, 1060–1067. [[CrossRef](#)]
70. Anirudhan, T.; Sreekumari, S. Adsorptive removal of heavy metal ions from industrial effluents using activated carbon derived from waste coconut buttons. *J. Environ. Sci.* **2011**, *23*, 1989–1998. [[CrossRef](#)]